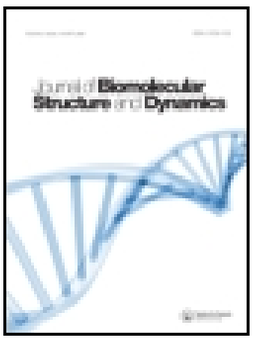

Journal of Biomolecular Structure and Dynamics

ISSN: (Print) (Online) Journal homepage: https://www.tandfonline.com/loi/tbsd20

Synthesis, characterization, antiproliferative of pyrimidine based ligand and its Ni(II) and Pd(II) complexes and effectiveness of electroporation

Mehmet Eşref Alkış , Kenan Buldurun , Nevin Turan , Yusuf Alan , Ünzile Keleştemur Yılmaz & Asim Mantarcı

To cite this article: Mehmet Eşref Alkış , Kenan Buldurun , Nevin Turan , Yusuf Alan , Ünzile Keleştemur Yılmaz & Asim Mantarcı (2020): Synthesis, characterization, antiproliferative of pyrimidine based ligand and its Ni(II) and Pd(II) complexes and effectiveness of electroporation, Journal of Biomolecular Structure and Dynamics, DOI: 10.1080/07391102.2020.1852965

To link to this article: https://doi.org/10.1080/07391102.2020.1852965

JOURNAL OF BIOMOLECULAR STRUCTURE AND DYNAMICS
https://doi.org/10.1080/07391102.2020.1852965

Taylor & Francis
Taylor & Francis Group

Synthesis, characterization, antiproliferative of pyrimidine based ligand and its Ni(II) and Pd(II) complexes and effectiveness of electroporation

Mehmet Eşref Alkış[a], Kenan Buldurun[b], Nevin Turan[c], Yusuf Alan[d], Ünzile Keleştemur Yılmaz[a] and Asim Mantarcı[e]

[a]Department of Occupational Health and Safety, Faculty of Health Sciences, Muş Alparslan University, Muş, Turkey; [b]Department of Food Processing, Technical Sciences Vocational School, Muş Alparslan University, Muş, Turkey; [c]Department of Chemistry, Faculty of Arts and Sciences, Muş Alparslan University, Muş, Turkey; [d]Department of Primary Education, Education Faculty, Muş Alparslan University, Muş, Turkey; [e]Department of Physics, Faculty of Arts and Sciences, Muş Alparslan University, Muş, Turkey

Communicated by Ramaswamy H. Sarma

ABSTRACT

In the study, a new Schiff base (ligand) was obtained using 4-aminopyrimidine-2(1*H*)-one, the starting material, and 2,3,4-trimethoxy benzaldehyde. Ni(II) and Pd(II) complexes were obtained from the reaction of the ligand and $NiCl_2{\cdot}6H_2O$, $PdCl_2(CH_3CN)_2$ (1:1 ratio). These compounds were characterized using the elemental and mass analysis, ^{1}H, ^{13}C-NMR, FT-IR, UV-Vis, magnetic susceptibility, thermal analysis, and the X-ray diffraction analyses. The antiproliferative activities of the synthesized ligand, Ni(II) and Pd(II) complexes were identified on the HepG2 (human liver cancer cells) cell line and their biocompatibility was tested on the L-929 (fibroblast cells) cell line by the MTT analysis method. Furthermore, the effects of electroporation (EP) on the cytotoxic activities of synthesized compounds were investigated in HepG2 cancer cells. According to the MTT findings of the study, the ligand did not exhibit an antiproliferative activity while its Ni(II) and Pd(II) complexes exhibited an antiproliferative activity. Moreover, it was observed that the antiproliferative activity of the Pd(II) complex was stronger than that of the Ni(II) complex. The combined application of EP + compounds is much more effective than the usage of the compounds alone in the treatment of HepG2 cancer cells. The EP increased the cytotoxicity of the Ni(II) and Pd(II) complexes by 1.66, and 2.54 times, respectively. It was concluded that Ni(II) and Pd(II) complexes may contribute as potential anti-cancer agents for the treatment of hepatocellular carcinoma and yield promising results in the case of being used in ECT.

ARTICLE HISTORY
Received 21 August 2020
Accepted 15 November 2020

KEYWORDS
Antiproliferative; cytotoxicity; electroporation; metal complexes; Schiff base

1. Introduction

Schiff bases exhibited significant effects in medical and pharmaceutical fields due to various biological activities (e.g. anti-inflammatory, analgesic, antimicrobial, anticonvulsant, antituberculosis, anticancer, antioxidant, anthelmintic) (Al-Humaidi, 2019; Buldurun et al., 2020). Schiff bases are highly preferred ligands in transition metal chemistry due to their ability to stabilize metals in different oxidation states (Alothman et al., 2020; Fekri et al., 2019). The most important source of biological effects is undoubtedly (CH = N) azomethine group. The nitrogen atom of the azomethine group plays an important role in the formation of hydrogen bonds with the active centers of the cell components and interfere with normal cell processes (Bingöl & Turan, 2020; Vashi & Naik, 2004). In addition to biological activities, Schiff bases are used as catalysts, intermediates in organic synthesis, dyes and in various material science fields (e.g. imaging systems and optical memory devices) (Dehghani-Firouzabadi & Firouzmandi, 2016; Geeta et al., 2010; Jain et al., 2020; Tahir et al., 2019; Yeğiner et al., 2017). Schiff bases and their transition metal complexes have potential biomedicine and biochemistry applications due to their successful biological system models and unique properties (Bernadette Amali et al., 2019; Zoubi, 2013). Schiff bases and their complexes can be easily obtained using mild reaction conditions and short reaction times, as well as thermodynamically and weather resistant compounds that exhibit interesting electronic and/or magnetic properties (Fetoh et al., 2019; Qin et al., 2013). Recently, many pyrimidine-containing compounds and their derivatives are reported to exhibit anticancer activity through interaction with different enzymes and receptors (Rahmouni et al., 2016; Rashad et al., 2011).

Hepatocellular carcinoma is the sixth most common cancer diagnosed worldwide (Emam et al., 2019) and ranks the third in the mortal cancer cases (Jemal et al., 2011). In general, radiotherapy, surgery, and chemotherapy drug treatment are the conventional methods used in the treatment of cancer (Levitsky & Dembitsky, 2015). Chemotherapy is a treatment method in which the cytotoxic drugs are used to prevent or eliminate the proliferation of cancer cells. Hepatocellular carcinoma, by its very nature, resists most of

CONTACT Mehmet Eşref Alkış me.alkis@alparslan.edu.tr Department of Occupational Health and Safety, Faculty of Health Sciences, Muş Alparslan University, Muş 49250, Turkey

Supplemental data for this article can be accessed online at https://doi.org/10.1080/07391102.2020.1852965.

the chemotherapeutic agents. Therefore, high-dose cytotoxic drugs with many side effects are being used in the treatment of hepatocellular carcinoma. Because of these reasons, there is a need for developing different therapeutic drugs and treatment methods for hepatocellular carcinoma.

Electroporation (EP) is a physical method in which the short-duration and high-strength electric pulses are applied to the cells or tissues and nanometer-sized transient pores are formed on the cell membranes. Thanks to the increase of cell membrane permeability poor permeable or nonpermeable molecules (e.g. DNA, RNA, drugs, dyes and antibodies) enter into the cell (Gehl, 2003; Neumann et al., 1982). This method was initially used for the gene transfer into cells; however, recently, it has been started to be applied in the transfer of various anti-cancer drugs into the cell (Cemazar & Sersa, 2019). The chemotherapy treatment carried out using the EP technique is called Electrochemotherapy (ECT). This treatment technique is efficient for cutaneous and subcutaneous cancers in humans and is now being used in the treatment of internal tumors (Vásquez et al., 2015). ECT makes it possible to provide treatment with a lower dose of the chemotherapeutic drugs by means of facilitating the delivery of anti-cancer drugs to the cell, thereby reducing the side effects of the drugs (Michel et al., 2018). The EP efficiency varies depending on the conditions such as electric field strength, cell concentration, type and duration of the current, temperature, and electroporation fluid (Batista Napotnik & Miklavčič, 2018). The optimum EP conditions were determined for the HepG2 cell line examined in this study by applying electric currents at different voltages. EP is more effective on the cancer cells than the healthy cells in terms of triggering cell death. The possible reason for this is the factors that differentiate the cancer cells from the healthy ones, such as different membrane compositions, membrane repair capacities, and energy reserves (Frandsen et al., 2016; Zielichowska et al., 2016).

Many researchers have carried out studies on different Schiff bases and metal complexes to develop new, safe, and effective chemotherapeutic agents (Arafath et al., 2017; Mohamed et al., 2019). However, although they examined the anti-cancer properties of the Schiff base and metal complexes they synthesized, they did not examine the effectiveness of the methods that would facilitate the delivery of molecules to the cancer cells, such as ECT. One of the main purposes of this study is to examine the effect of EP on the antiproliferative activities of synthesized compounds. A new type of pyrimidine Schiff base ligand and its Ni(II) and Pd(II) complexes were successfully synthesized and characterized in this work. Ligand and its metal complexes were characterized using different spectral methods (e.g. ^{1}H NMR, ^{13}C NMR, FT-IR, UV–Vis TGA, X-ray diffraction analysis, mass spectra and microanalysis). The cytotoxic activities of the synthesized compounds were studied against the cancer cell line (HepG2) and a normal cell line (L-929). Finally, the effects of EP on the cytotoxic activities of synthesized compounds were investigated in HepG2 cancer cells.

2. Materials and methods

2,3,4-trimethoxy benzaldehyde, 4-aminopyrimidine-2-(1*H*)-one (gemcitabine), $NiCl_2{\cdot}6H_2O$, $PdCl_2(CH_3CN)_2$ and ethanol, dimethyl sulphoxide (DMSO), dichloromethane, acetone, dimethylformamide (DMF), chloroform, methanol, diethyl ether used in this study were purchased from Sigma-Aldrich and used without purification. FT-IR spectra were performed on a Perkin Elmer (FT-IR model 65 spectrophotometer in the region 4000–400 cm^{-1} using KBr pellets). The NMR (^{1}H and ^{13}C) spectra were mentioned on a Bruker 300 MHz spectrometer in DMSO-d_6 as the solvent. The microanalysis (C, H, N) was performed by using a Vario III CHN analyzer. Mass spectra were performed on an Agilent technologies AB Sciex 3200 QTrap spectrometer. X-ray diffraction analysis was performed by an UltimaIV X-ray diffractometer with Rigaku (CuKα = 1.540562 A°). UV-Visible spectra were recorded in EtOH by used Shimadzu UV-1800 spectrophotometer. Thermogravimetric analysis (TGA) was monitored through a Universal TGA Q50 instrument (a heating rate of 10 °C/min between 50 and 900 °C).

The followings were used in the chemotherapy and ECT: Dimethylsulfoxide (DMSO), ethanol, fetal bovine serum (FBS) [PAN-Biotech, Europe], MTT [3-(4,5-dimethyl-2-thiazolyl)-2,5-diphenyl-2H-tetrazolium bromide] (AppliChem, Germany), Penicillin-Streptomycin (Sigma, USA), RPMI-1640 medium (Sigma, USA), Trypan blue (Sigma, USA), Trypsin-EDTA (Biological Industries, Israel), and Propidium iodide (PI). In all the experiments carried out on the HepG2 and L-929 cells, the cells between passages 8 and 12 were used. The cells used in the experiments were obtained from the Department of Biochemistry, Faculty of Arts and Science, Inonu University. The cells were incubated in a 5% CO_2 incubator (Esco, Singapore) at a temperature of 37 °C and a humidity of 95%. The cell culture work was carried out using a biosafety cabinet (ESCO, USA) under sterile conditions. Gene Pulser Xcell ™ (Bio-Rad, Hercules, CA, USA), 4 mm EP cuvettes (Bio-Rad, Hercules, CA, USA), and flow cytometry (Becton-Dickinson) were used for ECT.

2.1. Synthesis and characterization of Schiff base (4-(2,3,4-trimethoxy benzylidene)amino)pyrimidine-2-(1H)-on) (L)

The Schiff base (L) was prepared through refluxing methanol solution of 4-aminopyrimidine-2-(1*H*)-one (1.0 g; 1.0 mmol) with 2,3,4-trimethoxy benzaldehyde (1.76 g; 1.0 mmol) in methanol for 4 h and then allowed to cool. The white color crude product was washed methanol and dried at room temperature.

Schiff base (L): White solid, yield 80%, m.p.: 270 °C. Anal. calc. for $C_{14}H_{15}N_3O_4$ (FW: 289.29 g/mol) (%): C; 58.07, H; 5.18, N; 14.51. Found: C; 58.16, H; 5.30, N; 14.62. FT-IR (KBr, v max (cm^{-1})): 3176 (NH), 3097 (Ar–CH), 2899 (Al–CH), 1732 (C = O), 1662 (CH = N), 1632 (C = N), 1541, 1518, 1478 (C = C), 1100 (OCH_3). ^{1}H-NMR (300 MHz, DMSO-d_6, ppm) = 8.10 (s, H, NH), 8.48 (s, H, N = CH), 7.93–6.50 (m, 4H, Ar-H), 3.80–3.60 (s, 9H, OCH_3). ^{13}C-NMR (100 MHz, DMSO-d_6, ppm) = 162.45 (CH = N), 158.59 (C = N), 157.90 (C = O), 151.65–103.51 (Ar-C),

61.63–56.00 $(OCH_3)_3$. UV-Vis. (λ max/nm): 210, 220, 232, 249, 266, 274, 282, 295, 302, 360.

2.2. Synthesis of nickel and palladium complexes

In a 100 mL round bottom flask, the Schiff base ligand (0.40 g, 1.38 mmol) was dissolved in methanol (20 mL). A solution of $NiCl_2{\cdot}6H_2O$ and $PdCl_2(CH_3CN)_2$ (0.33 g, 1.38 mmol and 0.35 g, 1.38 mmol) in 20 mL of methanol was added to the mixture, the reaction mixture was refluxed for 6 h. The completion of the complexing reaction was checked by TLC and then let it be cool. The precipitate formed was filtrated. The product was washed with diethyl ether and dried.

$[NiCl_2L(H_2O)]{\cdot}2H_2O$: Green solid, yield 72%, m.p.: >270 °C. μ_{eff} (B.M.): 2.78. Anal. calc. for $C_{14}H_{21}N_3O_7NiCl_2$ (FW: 472.82 g/mol): C; 35.53, H; 4.44, N; 8.88. Found: C; 35.60, H; 4.56, N; 8.94. FT-IR (KBr, v max (cm^{-1})): 3320 (OH), 3176 (NH), 3097 (Ar–CH), 2982 (Al–CH), 1730 (C = O), 1656 (CH = N), 1636 (C = N), 1566, 1501, 1446 (C = C)Ar, 1094 (OCH_3), 800 (H_2O), 599, 546, 529 (M–O), 461 (M–N). UV–Vis. (λ max/nm): 219, 227, 237, 249, 278, 287, 357, 369, 484, 516. MS [ESI]: m/z 473.82 (Calc.), 473.39 (Found) $[M+H]^+$.

$[PdL(H_2O)]{\cdot}0.5H_2O{\cdot}Cl_2$: Cream solid, yield 74%, m.p.: >270 °C. μ_{eff} (B.M.): Dia, Anal. calc. for $C_{14}H_{18}N_3O_{5.5}PdCl_2$ (FW: 493.32 g/mol): C; 34.05, H; 3.64, N; 8.51. Found: C; 34.15, H; 3.60, N; 8.54. FT-IR (KBr, v max (cm^{-1})): 3424, 3310 (OH), 3178 (NH), 3096 (Ar–CH), 2886 (Al–CH), 1717 (C = O), 1670 (CH = N), 1633 (C = N), 1534, 1503, 1473 $(C=C)_{Ar}$, 1120 (OCH_3), 885 (H_2O), 579, 525 (M–O), 451 (M–N). ^{1}H-NMR (300 Mz, DMSO-d_6): δ (ppm) = 8.10 (s, H, NH), 8.32 (s, H, N = CH), 7.85–6.39 (m, 4H, Ar-H), 3.80–3.45 (s, 9H, OCH_3). ^{13}C-NMR (100 MHz, DMSO-d_6, ppm): 163.50 (CH = N), 159.28 (C = N), 153.43 (C = O), 151.18–103.03 (Ar-C), 61.90–52.18 $(OCH_3)_3$. UV–Vis. (λ max/nm): 219, 228, 235, 249, 256, 275, 387, 426. MS [ESI]: m/z 494.32 (Calc.), 494.96 (Found) $[M+H]^+$.

2.3. Antiproliferative activity

2.3.1. Cell culture experiments

The HepG2 and L-929 cells were used as models in the cell culture experiments. The development of the cells was examined under an inverted microscope daily. The cells were fed with the RPMI-1640 medium which was prepared by adding 10% FBS and 1% penicillin-streptomycin in 25 cm^2 culture flasks. The cells were incubated in a 5% CO_2 incubator at a temperature of 37 °C and a humidity of 95%.

2.3.2. Chemotherapy

The cells were counted using a cell counting device, and the viability was measured using the Trypan Blue Solution (0.4%). The experiments were not started in case the viability rate was below 90%. In the experiments, the cells were seeded in the 96-well plates at a density of 1×10^4 cells per well. The seeded cells were incubated for 24 h in an environment containing 5% CO_2 at 37 °C. After the medium liquids were removed from the incubated cells, 100 µL of the synthesized substance solutions prepared in medium (RPMI-1640) at the concentrations of 100, 200, 300, 400, and 500 µM were added to each well, and then the cells were again left for incubation for 24 h in an environment containing 5% CO_2 at 37 °C. The same concentrations were used for all samples in the MTT tests. Only 100 µL of medium (RPMI-1640) was added to the cells in the control wells (Aktaş et al., 2018; Sarı et al., 2020; Tan et al., 2020).

2.3.3. Determining the optimum electroporation conditions

It is of prime importance to monitor the permeability of the cells before proceeding to the electroporation application (Emam et al., 2019). In this study, propidium iodide (PI) was used to determine the cell electropermeabilization. 10 µL PI and 90 µL cell suspension (1×10^6 cell/mL) were added to the 4 mm EP cuvettes (Bio-Rad, Hercules, CA, USA) and then the cuvettes were placed in the EP device for the electrical pulse application. 8 square-wave pulse trains having various electric field strengths (375, 625, 875, 1125, and 1250 V/cm) with a duration of 100 µs and a frequency of 1 Hz were applied to the cell suspensions in order to determine the optimum electroporation conditions for the HepG2 cells to be used in the study. The control cells were also placed in the cuvettes under the same conditions, but the electric field was not applied to them. Following the EP, the cells were incubated with PI for 15 min at room temperature and then the percentage of permeabilized cells was measured using the flow cytometry (Becton-Dickinson). At least 10,000 cells were measured from each sample. The percentage of stained cells was found by making a comparison with the non-electroporated control cells. The electropermeabilization alone is not sufficient to determine the most appropriate electric field to be used in ECT. In addition to the best permeability, it is also important to determine the voltage causing the least cell death. For this purpose, 400 µL cell suspension (1×10^6 cell/mL) were placed in the 4 mm EP cuvettes without adding any agent or PI, and then the same voltages as in the electropermeabilization were applied. The HepG2 cells were examined in terms of both short-term (20-minute incubation after EP) and long-term (24 h incubation after EP) cell viability. The electroporation parameters were optimized for high permeability and low cellular mortality based on the MTT and PI analyses.

2.3.4. Electrochemotherapy (ECT)

When the HepG2 cells incubated to be used in the study reached a confluency of 80–90%, they were removed using 1X Trypsin-EDTA, and then the cell solution was transferred into falcon tubes and sedimented by centrifugation at 1000 rpm for 5 min. 400 µL cell suspension at a density of 1×10^6 cell/mL was transferred to the 4 mm EP cuvettes in a way that the concentration of each compound was at 200 µM. The cuvettes were placed in the Gene Pulser Xcell™ (Bio-Rad, Hercules, CA, USA) for the electric field application. Eight square-wave pulse trains having a strength of 1125 V/cm with a duration of 100 µs and a frequency of 1 Hz, which correspond to the parameters used in ECT clinical practice (Campana et al., 2019), were applied to the cell suspensions. Likewise, the control cells were placed in the

cuvettes under the same conditions, but the electric field was not applied to them. The experiments were repeated three times. 10–15 min after the EP, the cells were seeded in the 24-well cell culture plates and left for incubation. After 24 h incubation, the viability of the experimented cells was evaluated using the MTT analysis method.

2.3.5. MTT test (cytotoxicity test)

MTT [3-(4,5-dimethylthiazol-2-yl)-2,5-diphenyltetrazolium bromide] test was carried out to determine the cytotoxicity of the solutions of the synthesized substances prepared at different concentrations. For this purpose, the solution with a concentration of 5 mg/mL (60 mg MTT powder in 12 mL PBS) was covered with aluminum foil and left at +4 °C until the time it would be used. The plates, which were left for incubation after adding the substances, were taken and the medium in the wells was removed. Then, 10 µL MTT solution and 90 µL RPMI-1640 were added to each well and the plates were left for incubation for 4 h at 37 °C in an incubator containing 5% CO_2. After the 4 h of incubation, the medium containing MTT was removed and 100 µl DMSO was added to each well to dissolve the formazan crystals formed due to MTT reduction, and their optical density (OD) was measured at the wavelength of 570 nm (Mahajan et al., 2012) using a microplate reader. Only the fresh medium was used in the control group. The control wells were read and then the absorbance values obtained by reading were averaged. This value was accepted as 100% viable cell. The absorbance values read from the wells, to which the solutions of the synthesized substances were added, were proportioned to the absorbance value of the control group and calculated as percent viability using the following formula.

$$\% \text{ Viability} = (\text{OD of the group being examined} / \text{OD of the control group}) \times 100$$

The substance concentration yielding 50% inhibition (IC_{50}) was determined by the calculation carried out on the graph of the percentage of inhibition plotted against the substance concentration. The lower the IC_{50} value, the higher the anti-cancer capacity. All the analyzes were carried out in three parallel replicates, and each parallel experiment was repeated 6–8 times. The results were expressed as mean and standard deviation.

2.3.6. Statistical analysis

Statistical analyzes were performed by Graph Pad Prism software (Graph Pad Software Inc., San Diego, USA). Data were analyzed by one-way ANOVA followed by Dunnett's multiple comparisons test, or by Unpaired Parametric two-tailed t test where it was appropriate. $p < 0.05$ was considered to be statistically significant.

3. Result and discussion

3.1. IR spectra

The FT-IR spectrum of ligand refers to the band ν(CH = N) group assigned at 1662 cm^{-1}. This band was altered to different frequencies for the two complexes showing the involvement of the CH = N group in the complexation. In the IR spectrum of the ligand, the band observed at 3176 cm^{-1} was attributed to the ν(NH) group. The ν(NH) band appeared in the same position for the complexes and it showed that this group was not involved in complexing. The band showed at 1632 cm^{-1} was due to the ν(C = N) structure of the pyrimidine group of the ligand. This group did not change in Pd(II) complex. The band of $\nu(OCH_3)$ of the ligand seen at 1100 cm^{-1} was shifted to 1094 cm^{-1} and 1120 cm^{-1} for the Ni(II), Pd(II) complexes, respectively. This indicated that OCH_3 group was involved in chelation for the complexes. These observations were supported by new bands that appeared at 525–599 cm^{-1} and 451–461 cm^{-1} assigned to ν(M–O) and ν(M–N), respectively. All complexes exhibited a wide absorption band in the ranges of 3424–3310 cm^{-1} and 885–800 cm^{-1} relatives to the of hydration water molecules and the coordination water attached to metal(II) ions (Ali, 2017; Gomathi & Gopalakrishnan, 2016; Turan et al., 2019; Yeğiner et al., 2017) (Figure 1).

3.2. ^{1}H-NMR

The signal at 8.48 ppm corresponding to the CH = N resonance of the azomethine group in the ^{1}H NMR spectrum of the ligand shifted to 8.38 ppm in the spectra of the Pd(II) complex. This shift confirmed that the Schiff base was coordinated to Pd(II) ion as a chelating ligand. Signals observed in the ligand at 3.80–3.60 ppm were attributed to the OCH_3 group. These signals shifted to 3.80–3.45 ppm in the spectra of the Pd(II) complex. Shifting at signals to the high area for Pd(II) complex is evidence for the coordination of nitrogen atom of imine (CH = N) group and oxygen atom of methoxy (OCH_3) group to metal centers (Ali, 2014; Kargar et al., 2020).

3.3. UV-visible spectroscopy

The electronic spectrum of the Schiff base ligand in ethanol is due to bands $\pi \rightarrow \pi^*$ transitions at 220, 249, 266 and 282 nm. It showed a shoulder at 360 nm and a strong band at 302 nm due to the n$\rightarrow \pi^*$ transition of the non-common electrons found in the nitrogen of the azomethine group on the Schiff base. The $\pi \rightarrow \pi^*$, n$\rightarrow \pi^*$ transitions were shifted after the metal ions were coordinated towards the Schiff base ligand, this change supports that the nitrogen and oxygen atoms of the azomethine, carbonyl and pyrimidine group in the ring participate in coordination towards the metal ions. Spectral bands appearing at 227, 237, 249, 278, 287, 357, 369, 484 and 516 nm can be ascribed to the $\pi\rightarrow \pi^*$, n$\rightarrow \pi^*$ and MLCT transitions that support octahedral geometry, respectively (Saad, 2014; Shah et al., 2016; Yeğiner et al., 2017). The magnetic moment of the Ni(II) complex was found as 2.78 B.M. Palladium complex originates from two absorption bands d $\rightarrow$ d transitions observed at 387 nm and 426 nm in the UV spectrum. Electronic spectral results proposed that the Pd(II) complex had diamagnetic behavior and

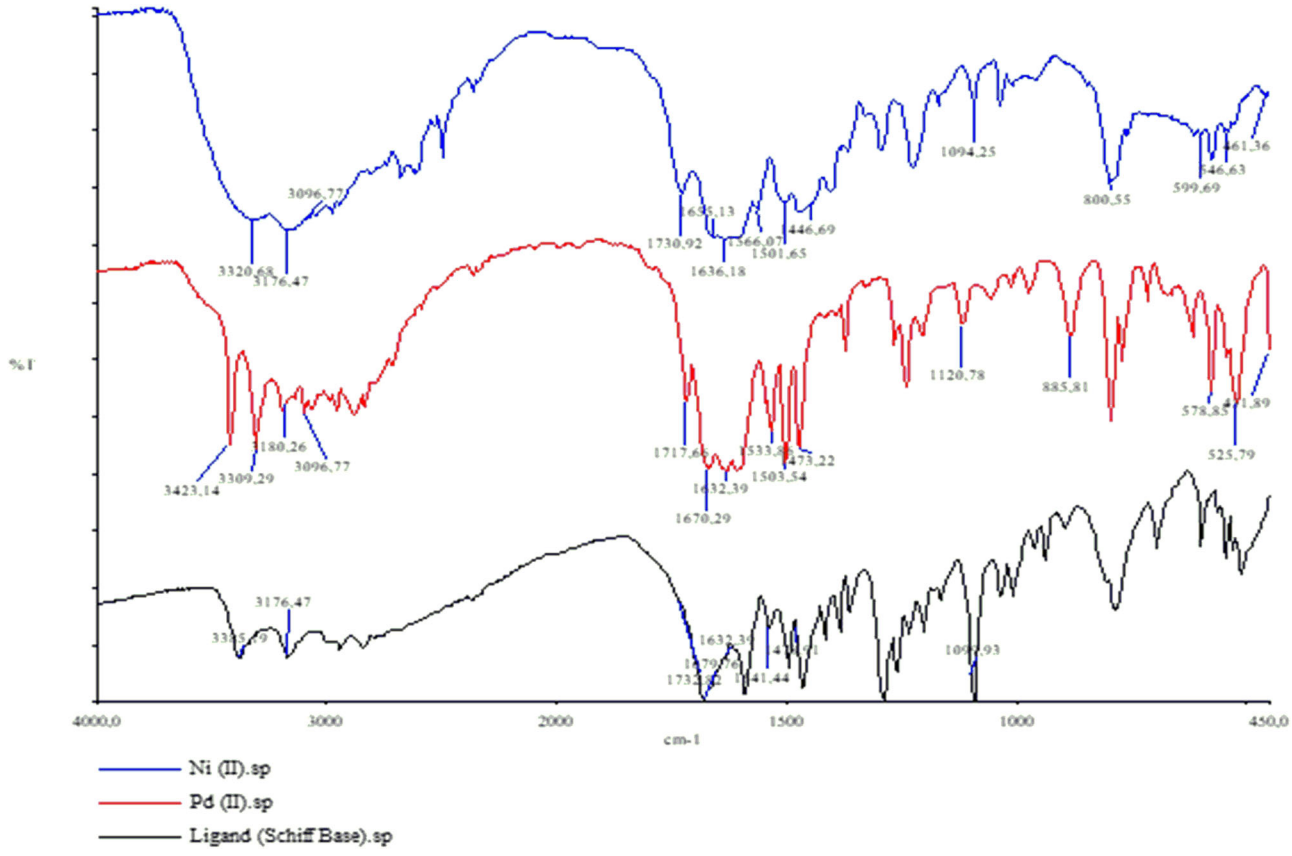

Figure 1. The FTIR spectrum of the compounds.

square planar geometry (Ali, 2017; Kumari et al., 2012; Yeğiner et al., 2017).

3.4. TGA analyses

The result of TGA analyses showed that spectral analyses were coherent with the theoretical formulae. $[NiCl_2L(H_2O)]\cdot 2H_2O$ complex decomposed in four stages. Its thermogram indicated a weight loss of 14.80% between 50 and 180 °C. This indicated the loss of three coordinated/hydration water molecules and one O atom of the carbonyl group. The second and third stages showed a weight loss of 48.20% (34.66% and 13.54%) in the 180–600 °C proving to the loss of $C_4H_3N_3Cl_2$, $C_2H_6O_2$ organic moiety. The remaining part of the complex decomposed in the fourth step between 600 and 790 °C with a loss of 24.95% leaving behind Ni metal ion. The $[PdL(H_2O)]\cdot 0.5H_2O\cdot Cl_2$ complex decomposes in three stages. Its thermogram showed a weight loss of 5.47% in the 50–220 °C region confirming the loss of three coordinated/hydration water molecules. The second and third stages showed a weight loss of 69.70% (7.18% and 62.52%) in the 220–700 °C confirming the loss of Cl, $C_{14}H_{15}N_3O_3Cl$ organic moiety. The rest of the ligand decomposed at the fourth step for Pd(II) complex and metal oxide (PdO) remained as a residue (Ali, 2014; Buldurun et al., 2019; Gaber et al., 2019). The proposed stepwise decomposition pattern of $[NiCl_2L(H_2O)]\cdot 2H_2O$ and $[PdL(H_2O)]\cdot 0.5H_2O\cdot Cl_2$ complexes at different steps were due to the loss of different organic moieties with respect to temperature, which was showed in Table 1.

3.5. Powder X-ray diffraction analyses

UltimaIV X-ray diffractometer (Rigaku model with CuK_α=0.1540562 nm) was operated to measure the crystal structure of the complexes. XRD working conditions can be listed as follows; scan step: 0.02°, scanning range: 10–90°, scanning mode: 2Theta/Theta, scanning type: continuous scanning, operating current: 30 mA, operating voltage: 40 kV. XRD spectrums of Ni(II) and Pd(II) complexes are shown in Figure 2. Estimated crystal parameters (FWHM, grain size, detected diffraction angle) of these complexes are displayed in Table 2.

3.5.1. XRD results of Ni(II) complex

XRD phase behavior of the Ni(II) complex was given in Figure 2. The peak having high intensity was observed from XRD measurement. The peak detected diffraction angle and related intensity were 28.19° and ~357 (a.u), respectively. The orientation of the observed peaks cannot be given because the complex is synthesized for the first time and is not available in the literature. Some crystallographic parameters of a similar complex are referred to (Buldurun et al., 2019; Nithya et al., 2018). We estimated grain sizes of the complex with Scherer's equation;

$$K = \frac{r\lambda}{FCos\theta} \quad (1)$$

λ shows X-ray wavelength, θ shows Bragg's diffraction angle, $r = 0.94$ shows constant, F shows full width of half maximum intensity. The average grain sizes (K) of the complex were

Table 1. Thermal analysis of Ni(II) and Pd(II) complexes.

Compounds	Dissoc. stage	Decomp. temp. (°C)	Weight loss[%] calc. (found)		Decomp. assign.
$[NiCl_2L(H_2O)]\cdot 2H_2O$	1	50–180	14.86	14.80	$3H_2O$, O atom
	2	180–450	34.05	34.66	$C_4H_3N_3Cl_2$
	3	450–600	13.57	13.54	$C_2H_6O_2$
	4	600–790	25.03	24.95	C_8H_6O
Residue		>790	12.49	12.41	Ni metal
$[PdL(H_2O)]\cdot 0.5H_2O\cdot Cl_2$	1	50–220	5.38	5.47	$1.5H_2O$
	2	220–320	7.05	7.18	Cl
	3	320–700	61.25	62.52	$C_{14}H_{15}N_3O_3Cl$
Residue		>800	26.32	24.83	PdO

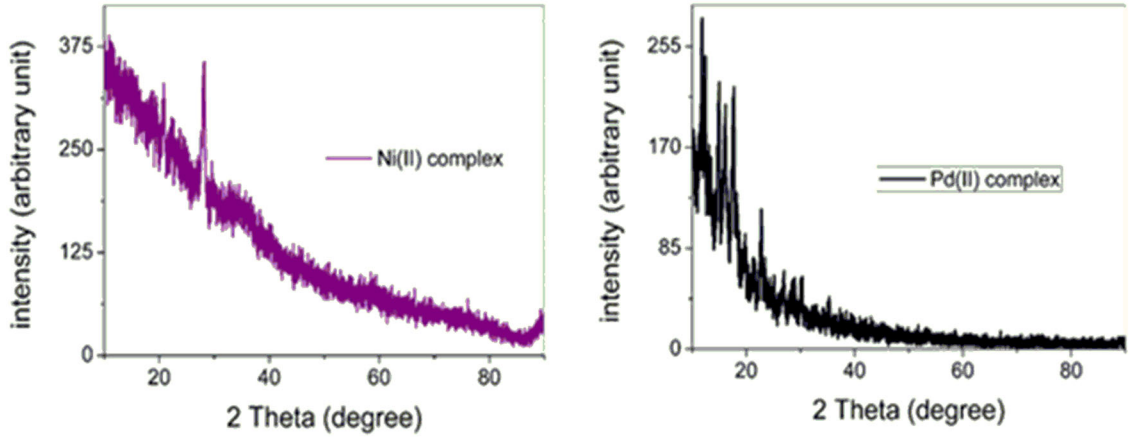

Figure 2. XRD behavior of Ni(II) and Pd(II) complexes.

Table 2. Grain sizes of the Pd(II) and Ni(II) complexes.

Compounds	2θ (°)	Full width half max. (F) (°)	Grain size (K)(nm)
Ni(II) complex	28.19	0.49	17.06
Pd(II) complex	11.8	0.26	31.95
	12.4	0.16	51.93
	15	0.39	21.32
	16.1	0.48	17.33
	17.7	0.34	24.48
	22.7	0.15	55.59

calculated from the highest peak intensity. Grain size values of the Ni(II) complex given in Table 2. The grain size of the related peak of the complex was found to be 17.06 nm.

3.5.2. XRD results of Pd(II) complex

XRD phase behavior of the Pd(II) complex was given in Figure 2. Several peaks having high intensities were detected from XRD. These peaks can be listed as follows; 11.8° (intensity 279 (a.u)), 12.4° (intensity 247 (a.u)), 15° (intensity 226 (a.u)), 16.1° (intensity 206 (a.u)), 17.7° (intensity 222 (a.u)), 22.7° (intensity 118 (a.u)). The highest intensity was found at the peak of 11.8°, while the lowest intensity was found at the peak of 22.7°. XRD measurement confirmed that this complex has a polycrystalline phase. The orientation of the detected peaks cannot be given because the complex is synthesized for the first time and is not available in the literature. Grain sizes of the complex were calculated with Scherer's equation (Equation (1)). Grain size values of the Pd(II) complex can be given in Table 2. Our results gave that the highest grain size was obtained at a 22.7° diffraction angle; the lowest one was obtained at a 16.1° diffraction angle. From XRD measurement, it was also detected weaker peaks at about 40°. It may be due to the diffraction peaks corresponding to the precursors.

3.6. Antiproliferative activity

The solutions of the synthesized ligand and its Ni(II) and Pd(II) complexes having five different concentrations (100, 200, 300, 400, and 500 μM) were treated with the HepG2 and L-929 cells for 24 h and their spectrophotometric absorbances were measured. The percent inhibition values of the HepG2 and L-929 cells were calculated with the measured absorbances. The inhibition occurring in the cell proliferation was determined by the MTT test. The IC_{50} values of the test substances were calculated in order to find out whether they had cytotoxic effects on the hepatocellular carcinoma and the mouse fibroblast cells (Table 3).

In this study, the IC_{50} values of the chemical test agents applied in vitro to the HepG2 and L-929 cells were analyzed. The higher the IC_{50} value, the lower the cytotoxicity. When the parameters measured in this study are analyzed, it can be asserted that the synthesized Ni(II) and Pd(II) complexes have the anti-cancer properties and the cytotoxicity of the Pd(II) complex is higher than the Ni(II) complex (Gaber et al., 2015). The geometry of the complex can affect its DNA binding and activity (Indumathy et al., 2008). The possible reason for the Ni(II) complex to exhibit a lower activity than the Pd(II) complex is the fact that its geometry is not planar. Furthermore, as can be understood from the IC_{50} values in Table 3, although the Pd(II) complex displayed a very high cytotoxic effect on the HepG2 cells, it displayed a very low cytotoxic effect on the L-929 cells.

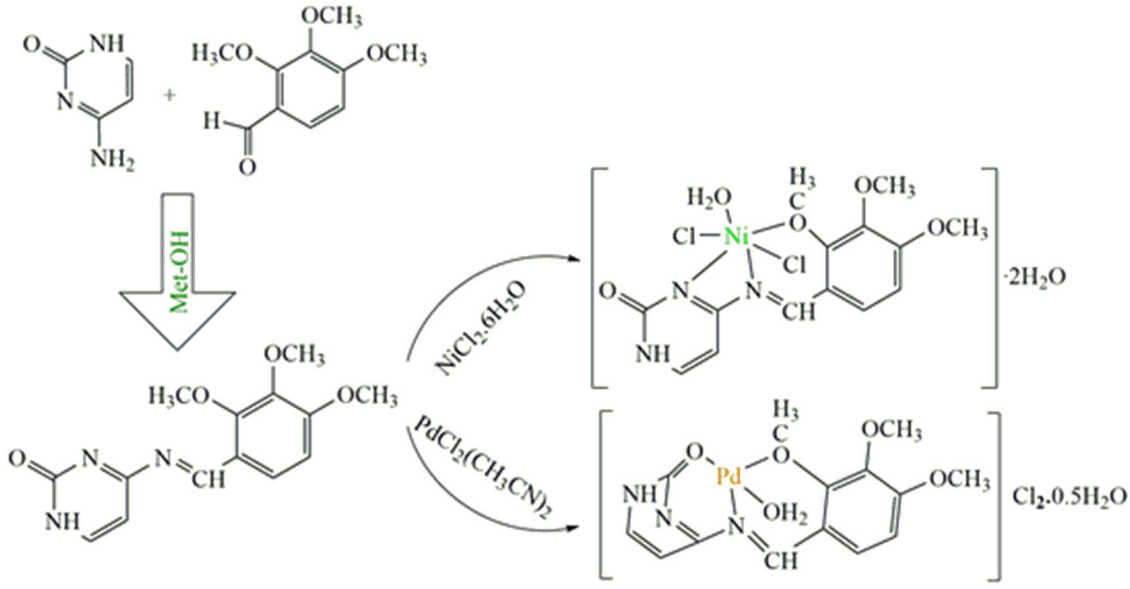

Scheme 1. Structure of Schiff base and its Ni(II), Pd(II) complexes.

Several studies have shown that Schiff base ligands, Ni(II) and Pd(II) complexes exhibit cytotoxicity in various cancer cells and tissues. Arafath et al. (2017) reported that the carbothioamide Schiff base ligand and its Ni(II), Pd(II) and Pt(II) complexes have strong cytotoxic property and selectivity against human cervical and colorectal tumor cells. Therefore, further studies are recommended as complexes derived from carbothioamide Schiff base could be promising chemotherapeutic agents against human malignancy. In another study, the cytotoxicity of chitosan, chitosan-Schiff base and Cu(II), Ni(II) and Zn(II) complexes was tested against K562 chronic myelogenous leukemia (CML) and MG-63 (osteosarcoma cancer) cell lines by the MTT assay. It is shown that the anticancer activity of Schiff base and complexes is much better than that of pure Chitosan against MG63 cancer cell line (Malekshah et al., 2020). In a study conducted by Şahin et al. (2018) the anti-cancer activity of the synthesized ligand, Pd(II) and Pt(II) complexes was evaluated in vitro on MCF-7 (human breast adenocarcinoma), LS174T (human colon carcinoma) and LNCAP (human prostate adenocarcinoma) cancer cell lines using the MTT assay. Based on the activity results, the Pd(II) complex has been shown to have higher anti-tumor effect than the ligand and its Pt(II) complex against the tested human breast adenocarcinoma, human prostate adenocarcinoma and human colon carcinoma cell lines. The findings obtained in our study are consistent with the results of the studies mentioned above.

3.7. Electropermeabilization and viability of the cells

The electropermeabilization of the HepG2 cells was measured by flow cytometry using PI. The permeability percentages of the cell membrane depending on various electric field strengths (0, 375, 625, 875, 1125, and 1250 V/cm) were given in Figure 3.

As can be seen in the Figure 3, as the magnitude of the electric fields increased, the permeabilization percentages of the cells also increased. However, drastic changes were observed in the permeability of the cells at 1125 V/cm. It was observed that the permeability of the HepG2 cells at this electric field strength was found to be approximately 59%. Moreover, the HepG2 cells were analyzed in terms of both short-term (20 min incubation after EP) and long-term (24 h incubation after EP) cell viability by means of applying the same electric fields used in the electropermeabilization.

Table 3. The IC_{50} values of the ligand and its Ni(II), Pd(II) complexes in the HepG2 and L-929 cells.

Compounds	Hep G2 IC_{50} (μM)	L-929 IC_{50} (μM)
L	989.62	866.57
Ni(II) complex	454.62	1622.73
Pd(II) complex	387.5	1224.44

While the short-term cell viability was measured using a cell counting device (Thermo scientific), the long-term cell viability was measured using the MTT test. As can be seen in the Figure 4 above, as the strength of the electric field pulses increased, a decrease was observed in the viability of the cells. After 1125 V/cm, sharp declines were observed in the cell viability. 20 min and 24 h after the electroporation, the viabilities of the cells were measured to be 52.5% and 69.57%, respectively, at 1125 V/cm. When the electropermeabilization and short- and long-term cell viability analyzes were evaluated together, it was found that the electric field strength of 1125 V/cm (100 μs, 1 Hz, 8 square waves) was appropriate for the electroporation as it exhibited a high permeability and low cellular mortality.

3.8. Efficacy of electroporation in treatment

8 square-wave pulse trains having a strength of 1125 V/cm with a duration of 100 μs and a repetition frequency of 1 Hz were used in the ECT. After the 24 h incubation, the cell viability percentages in the compound-alone and compound + EP groups

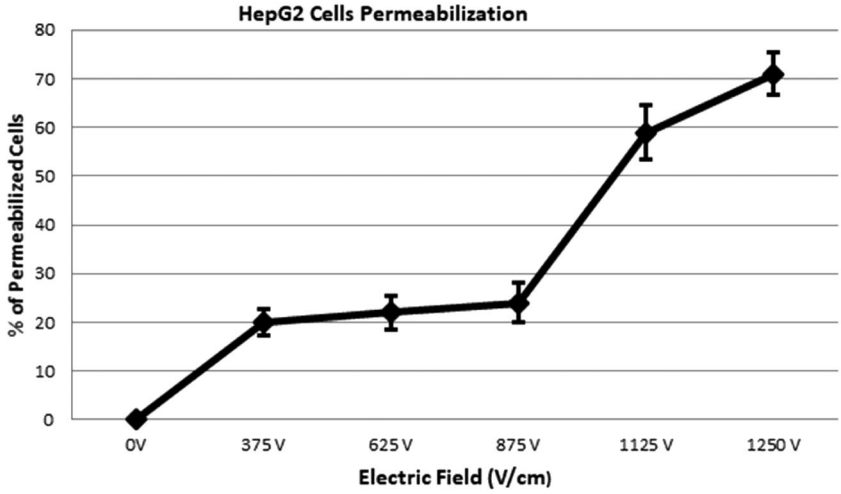

Figure 3. The permeabilization percentage of the HepG2 cells 20 min after the electroporation treatment. The data is given as the mean ± SD of three independent experiments.

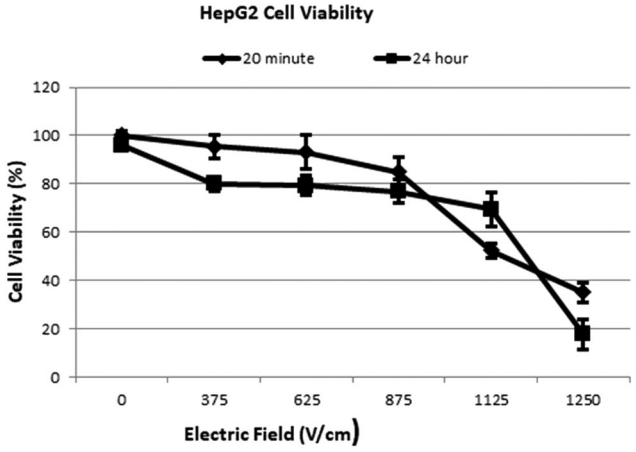

Figure 4. Cell viability of electroporated HepG2 cells at 20 min and 24 h after the electroporation. The data were taken from three independent experiments and presented as mean ± SD.

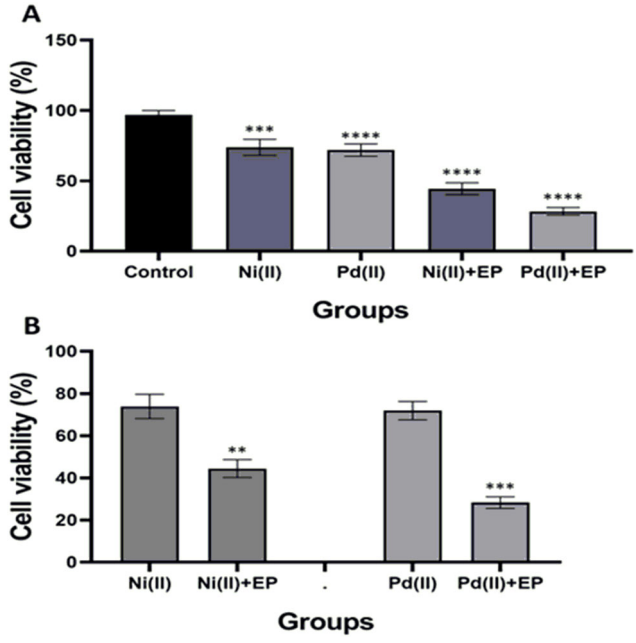

Figure 5. Cell viability of HepG2 cells at 24 h under different treatment conditions: Control, Ni(II) complex only, Pd(II) complex only, Ni(II) complex + EP and Pd(II) complex + EP treatment. (A) The treatment groups were compared with the control group using One Way ANOVA, Dunnett's multiple comparisons test. (B) Ni(II), Ni(II)+EP and Pd(II), Pd(II)+EP were compared among themselves using Unpaired Parametric two-tailed t test. A significant difference was found between groups at different levels (*$p < 0.05$, significant; **$p < 0.01$, very significant; ***$p < 0.001$ and ****$p < 0.0001$, extremely significant). The data were taken from three independent experiments and presented as mean ± SD.

were measured using the MTT analysis, and the data were given in the Figure 5.

There was a statistically significant decrease in MCF-7 cancer cells viability (%) of all treatment (Ni(II), Pd(II), Ni(II)+EP and Pd(II)+EP) groups compared to control group ($p < 0.05$). When the chemotherapy (Ni(II), Pd (II)) and electrochemotherapy (Ni(II) + EP, Pd(II) + EP) groups were compared, the difference between them was found to be statistically significant ($p < 0.05$) (Figure 5B). The antiproliferative activities of the Ni(II) and Pd(II) complexes significantly increased with the EP. When the two complexes were compared, it was found that the Pd(II) complex highly reduced the number of viable cells and so, displayed the best antiproliferative effect. As can be understood from the Figure 5, the synthesized compounds in general exhibited a more antiproliferative effect in the ECT than the standard chemotherapy. When the electric field pulses are applied to a cell, a transmembrane voltage is induced on the cell membrane (Zhang et al., 2010). If the voltage induced on the cell membrane exceeds a certain value, it causes a significant increase in the permeability and electrical conductivity of the membrane. With the help of the increased membrane permeability, the molecules that have large molecular structures and are otherwise difficult to deliver, such as nucleic acids, cytotoxic drugs, proteins, peptides, and ions, can be delivered across the membrane (Campana et al., 2019; Zhang et al., 2010). The possible main reason why the complexes synthesized in this study displayed a better antiproliferative activity with the help of EP is the fact that the EP increases the uptake of these complexes to the cell.

After the electric field exposure is applied at an appropriate amplitude (<1500 V/cm) and for an appropriate duration, the membrane returns to its normal state (reversible EP). On the other hand, if the amplitude of the electric field is too

high (1500–3000 V/cm) or if the duration of the electric field exposure is too long, the membrane does not close after the exposure and this causes cell death (irreversible EP) (Bharti et al., 2010). The reversible EP is being used for increasing the delivery of cytotoxic drugs in the local tumor treatment as well as being used in many fields such as DNA vaccination and gene therapy (Romeo et al., 2018). The optimum EP conditions (1125 V/cm, 100 μs, 1 Hz, 8 pulses) used in this study were determined based on the electropermeabilization analysis and the analyses carried out on the HepG2 cells to find out their electric field sensitivity at various electric field strengths.

ECT is highly effective even when used with low-dose chemotherapeutic agents, and it has become a standard treatment method for the therapy of the deep-seated tumors and the local cutaneous and subcutaneous metastatic tumors in different parts of the body. Recently, it has been applied in many clinics in Europe (Cadossi et al., 2014; Miklavčič et al., 2012). Today, ECT is being developed and evaluated for the treatment of subcutaneous tumors or internal organ tumors (Schneider et al., 1990). Mali et al. (2013) examined 44 studies on the effectiveness of ECT in the treatment of malignant melanomas, breast cancer, and head and neck tumors. They found that ECT yielded an objective response rate of 84.1% and a complete remission rate of 59.4%, regardless of tumor type. On the other hand, Esmekaya et al. (2016) reported that the electroporation increased the delivery of the anti-cancer drugs to the cells and decreased the minimum dosage required for treatment. Our findings are in parallel with the findings of these studies. It was found that, in the HepG2 cell line, the EP increased the cytotoxicity of the Ni(II) and Pd(II) complexes by 1.66, and 2.54 times, respectively, compared to applying only the metal complexes.

4. Conclusion

A new type of pyrimidine bases Schiff base ligand and its Ni(II) and Pd(II) complexes were successfully synthesized and characterized in this study. Ligand and its metal complexes were characterized using the elemental and mass analysis, ^{1}H-NMR, ^{13}C-NMR, FT-IR, UV-VIS, magnetic susceptibility, thermal analysis. In vitro antiproliferative activities of the compounds on the HepG2 human cancer cell line was performed by MTT assay. Furthermore, the effects of electroporation on the cytotoxic activities of synthesized compounds were investigated in HepG2 cancer cells. The results showed that the ligand did not exhibit an antiproliferative activity while its Ni(II) and Pd(II) complexes showed an antiproliferative activity and Pd(II) had stronger antiproliferative activity than Ni(II) against HepG2 cancer cells. The combined application of EP + compounds was much more effective than the usage of the compounds alone in the treatment of HepG2 cancer cells. EP increased the cytotoxicity of the compounds, therefore lower doses of compounds treatment with EP were as effective as higher doses for compounds treatment without EP. It was observed that the efficacy of ECT in treatment was quite high compared to the standard chemotherapy. It is expected that the results of this study contribute to new therapeutic studies for hepatocellular carcinoma.

Acknowledgements

This work is supported by the Scientific Research Project Fund of Muş Alparslan University under the project number BAP-18-MMF-4901-02.

Disclosure statement

The authors declare that no conflicts of interest.

ORCID

Mehmet Eşref Alkış http://orcid.org/0000-0002-3321-2873
Kenan Buldurun http://orcid.org/0000-0002-2462-7006
Nevin Turan http://orcid.org/0000-0001-6740-6812
Yusuf Alan http://orcid.org/0000-0003-0007-0212
Ünzile Keleştemur Yılmaz http://orcid.org/0000-0003-4531-6378
Asim Mantarcı http://orcid.org/0000-0001-8369-3559

References

Aktaş, A., Keleştemur, Ü., Gök, Y., Balcıoğlu, S., Ateş, B., & Aygün, M. (2018). 2-Morpholinoethyl-substituted N-heterocyclic carbene (NHC) precursors and their silver(I)NHC complexes: Synthesis, crystal structure and in vitro anticancer properties. *Journal of the Iranian Chemical Society*, *15*(1), 131–139. https://doi.org/10.1007/s13738-017-1216-8

Al-Humaidi, J. Y. (2019). In situ alkaline media: Synthesis, spectroscopic, morphology and anticancer assignments of some transition metal ion complexes of 1-((2-aminophenylimino) methyl) naphthalen-2-ol Schiff base. *Journal of Molecular Structure*, *1183*, 190–201. https://doi.org/10.1016/j.molstruc.2019.01.083

Ali, O. A. M. (2014). Synthesis, spectroscopic, fluorescence properties and biological evaluation of novel Pd(II) and Cd(II) complexes of NOON tetradentate Schiff bases. *Spectrochimica Acta. Part A, Molecular and Biomolecular Spectroscopy*, *121*, 188–195. https://doi.org/10.1016/j.saa.2013.10.015

Ali, O. A. M. (2017). Characterization, thermal and fluorescence study of Mn(II) and Pd(II) Schiff base complexes. *Journal of Thermal Analysis and Calorimetry*, *128*(3), 1579–1590. https://doi.org/10.1007/s10973-016-6055-9

Alothman, A. A., Al-Farraj, E. S., Al-Onazi, W. A., Almarhoon, Z. M., & Al-Mohaimeed, A. M. (2020). Spectral characterization, electrochemical, antimicrobial and cytotoxic studies on new metal(II) complexes containing N_2O_4 donor hexadentate Schiff base ligand. *Arabian Journal of Chemistry*, *13*(2), 3889–3902. https://doi.org/10.1016/j.arabjc.2019.02.003

Arafath, M. A., Adam, F., Razali, M. R., Ahmed Hassan, L. E., Ahamed, M. B. K., & Majid, A. M. S. A. (2017). Synthesis, characterization and anticancer studies of Ni(II), Pd(II) and Pt(II) complexes with Schiff base derived from N-methylhydrazinecarbothioamide and 2-hydroxy-5-methoxy-3-nitrobenzaldehyde. *Journal of Molecular Structure*, *1130*, 791–798. https://doi.org/10.1016/j.molstruc.2016.10.099

Batista Napotnik, T., & Miklavčič, D. (2018). In vitro electroporation detection methods - An overview. *Bioelectrochemistry (Amsterdam, Netherlands)*, *120*, 166–182. https://doi.org/10.1016/j.bioelechem.2017.12.005

Bernadette Amali, I., Kesavan, M. P., Vijayakumar, V., Indra Gandhi, N., Rajesh, J., & Rajagopal, G. (2019). Structural analysis, antimicrobial and cytotoxic studies on new metal(II) complexes containing N_2O_2 donor Schiff base ligand. *Journal of Molecular Structure*, *1183*, 342–350. https://doi.org/10.1016/j.molstruc.2019.02.005

Bharti, S. K., Nath, G., Tilak, R., & Singh, S. K. (2010). Synthesis, anti-bacterial and anti-fungal activities of some novel Schiff bases containing 2,4-disubstituted thiazole ring. *European Journal of Medicinal Chemistry*, *45*(2), 651–660. https://doi.org/10.1016/j.ejmech.2009.11.008

Bingöl, M., & Turan, N. (2020). Schiff base and metal(II) complexes containing thiophene-3-carboxylate: Synthesis, characterization and antioxidant activities. *Journal of Molecular Structure*, *1205*, 127542. https://doi.org/10.1016/j.molstruc.2019.127542

Buldurun, K., Turan, N., Aras, A., Mantarcı, A., Turkan, F., & Bursal, E. (2019). Spectroscopic and structural characterization, enzyme inhibitions, and antioxidant effects of new Ru(II) and Ni(II) complexes of Schiff base. *Chemistry & Biodiversity*, *16*(8), e1900243. https://doi.org/10.1002/cbdv.201900243

Buldurun, K., Turan, N., Bursal, E., Aras, A., Mantarcı, A., Çolak, N., Türkan, F., & Gülçin, İ. (2020). Synthesis, characterization, powder X-ray diffraction analysis, thermal stability, antioxidant properties and enzyme inhibitions of M(II)-Schiff base ligand complexes. *Journal of Biomolecular Structure and Dynamics*. https://doi.org/10.1080/07391102.2020.1802340

Cadossi, R., Ronchetti, M., & Cadossi, M. (2014). Locally enhanced chemotherapy by electroporation: Clinical experiences and perspective of use of electrochemotherapy. *Future Oncology*, *10*(5), 877–890. https://doi.org/10.2217/fon.13.235

Campana, L. G., Miklavčič, D., Bertino, G., Marconato, R., Valpione, S., Imarisio, I., Dieci, M. V., Granziera, E., Cemazar, M., Alaibac, M., & Sersa, G. (2019). Electrochemotherapy of superficial tumors - Current status: Basic principles, operating procedures, shared indications, and emerging applications. *Seminars in Oncology*, *46*(2), 173–191. https://doi.org/10.1053/j.seminoncol.2019.04.002

Cemazar, M., & Sersa, G. (2019). Recent advances in electrochemotherapy. *Bioelectricity*, *1*(4), 204–213. https://doi.org/10.1089/bioe.2019.0028

Dehghani-Firouzabadi, A., & Firouzmandi, S. (2016). Synthesis and characterization of a new unsymmetrical potentially pentadentate Schiff base ligand and related complexes with manganese(II), nickel(II), copper(II), zinc(II) and cadmium(II). *Journal of the Brazilian Chemical Society*, *28*, 768–774. https://doi.org/10.21577/0103-5053.20160226

Emam, M. A., Khattab, H. I., & Hegazy, M. G. (2019). Assessment of anticancer activity of pulicaria undulata on hepatocellular carcinoma HepG2 cell line. *Tumour Biology*, *41*(10), 1010428319880080. https://doi.org/10.1177/1010428319880080

Esmekaya, M. A., Kayhan, H., Coskun, A., & Canseven, A. G. (2016). Effects of cisplatin electrochemotherapy on human neuroblastoma cells. *The Journal of Membrane Biology*, *249*(5), 601–610. https://doi.org/10.1007/s00232-016-9891-4

Fekri, R., Salehi, M., Asadi, A., & Kubicki, M. (2019). Synthesis, characterization, anticancer and antibacterial evaluation of Schiff base ligands derived from hydrazone and their transition metal complexes. *Inorganica Chimica Acta*, *484*, 245–254. https://doi.org/10.1016/j.ica.2018.09.022

Fetoh, A., Asla, K. A., El-Sherif, A. A., El-Didamony, H., & Abu El-Reash, G. M. (2019). Synthesis, structural characterization, thermogravimetric, molecular modelling and biological studies of Co(II) and Ni(II) Schiff bases complexes. *Journal of Molecular Structure*, *1178*, 524–537. https://doi.org/10.1016/j.molstruc.2018.10.066

Frandsen, S. K., McNeil, A. K., Novak, I., McNeil, P. L., & Gehl, J. (2016). Difference in membrane repair capacity between cancer cell lines and a normal cell line. *The Journal of Membrane Biology*, *249*(4), 569–576. https://doi.org/10.1007/s00232-016-9910-5

Gaber, M., El-Ghamry, H. A., & Fathalla, S. K. (2015). Ni(II), Pd(II) and Pt(II) complexes of (1H-1,2,4-triazole-3-ylimino)methyl]naphthalene-2-ol. Structural, spectroscopic, biological, cytotoxicity, antioxidant and DNA binding. *Spectrochimica Acta. Part A, Molecular and Biomolecular Spectroscopy*, *139*, 396–404. https://doi.org/10.1016/j.saa.2014.12.057

Gaber, M., El-Wakiel, N., El-Baradie, K., & Hafez, S. (2019). Chromone Schiff base complexes: Synthesis, structural elucidation, molecular modeling, antitumor, antimicrobial, and DNA studies of Co(II), Ni(II), and Cu(II) complexes. *Journal of the Iranian Chemical Society*, *16*(1), 169–182. https://doi.org/10.1007/s13738-018-1494-9

Geeta, B., Shravankumar, K., Reddy, P. M., Ravikrishna, E., Sarangapani, M., Reddy, K. K., & Ravinder, V. (2010). Binuclear cobalt(II), nickel(II), copper(II) and palladium(II) complexes of a new Schiff-base as ligand: Synthesis, structural characterization, and antibacterial activity. *Spectrochimica Acta. Part A, Molecular and Biomolecular Spectroscopy*, *77*(4), 911–915. https://doi.org/10.1016/j.saa.2010.08.004

Gehl, J. (2003). Electroporation: Theory and methods, perspectives for drug delivery, gene therapy and research. *Acta Physiologica Scandinavica*, *177*(4), 437–447. https://doi.org/10.1046/j.1365-201X.2003.01093.x

Gomathi, G., & Gopalakrishnan, R. (2016). A hydrazone Schiff base single crystal (E)-methyl N(′)-(3,4,5-trimethoxybenzylidene) hydrazine carboxylate: Physicochemical, in vitro investigation of antimicrobial activities and molecular docking with DNA gyrase protein. *Materials Science & Engineering. C, Materials for Biological Applications*, *64*, 133–138. https://doi.org/10.1016/j.msec.2016.03.084

Indumathy, R., Kanthimathi, M., Weyhermuller, T., & Nair, B. U. (2008). Cobalt complexes of terpyridine ligands: Crystal structure and nuclease activity. *Polyhedron*, *27*(17), 3443–3450. https://doi.org/10.1016/j.poly.2008.08.003

Jain, P., Kumar, D., Chandra, S., & Misra, N. (2020). Experimental and theoretical studies of Mn(II) and Co(II) metal complexes of a tridentate Schiff's base ligand and their biological activities. *Applied Organometallic Chemistry*, *34*(2), e5371. https://doi.org/10.1002/aoc.5371

Jemal, A., Bray, F., Center, M. M., Ferlay, J., Ward, E., & Forman, D. (2011). Global cancer statistics. *CA: A Cancer Journal for Clinicians*, *61*(2), 69–90. https://doi.org/10.3322/caac.20107

Kargar, H., Torabi, V., Akbari, A., Behjatmanesh-Ardakani, R., Sahraei, A., & Tahir, M. N. (2020). Pd(II) and Ni(II) complexes containing an asymmetric Schiff base ligand: Synthesis, x-ray crystal structure, spectroscopic investigations and computational studies. *Journal of Molecular Structure*, *1205*, 127642. https://doi.org/10.1016/j.molstruc.2019.127642

Kumari, N., Yadav, V. K., Zalis, S., & Mishra, L. (2012). ChemInform abstract: Pd(II) catalyzed transformation of Schiff bases in complexes of the type trans-$[PdCl_2(NH_2Ar\text{-}X)_2]$ (X: H, CH_3, Cl). *ChemInform*, *43*(34), 554-563. https://doi.org/10.1002/chin.201234032

Levitsky, D. O., & Dembitsky, V. M. (2015). Anti-breast cancer agents derived from plants. *Natural Products and Bioprospecting*, *5*(1), 1–16. https://doi.org/10.1007/s13659-014-0048-9

Mahajan, S. D., Law, W.-C., Aalinkeel, R., Reynolds, J., Nair, B. B., Yong, K.-T., Roy, I., Prasad, P. N., & Schwartz, S. A. (2012). Nanoparticle-mediated targeted delivery of antiretrovirals to the brain. *Methods in Enzymology*, *509*, 41–60. https://doi.org/10.1016/B978-0-12-391858-1.00003-4

Malekshah, R. E., Shakeri, F., Khaleghian, A., & Salehi, M. (2020). Developing a biopolymeric chitosan supported Schiff-base and Cu(II), Ni(II) and Zn(II) complexes and biological evaluation as pro-drug. *International Journal of Biological Macromolecules*, *152*, 846–861. https://doi.org/10.1016/j.ijbiomac.2020.02.245

Mali, B., Jarm, T., Snoj, M., Sersa, G., & Miklavcic, D. (2013). Antitumor effectiveness of electro chemotherapy: A systematic review and meta-analysis. *European Journal of Surgical Oncology*, *39*(1), 4–16. https://doi.org/10.1016/j.ejso.2012.08.016

Michel, O., Kulbacka, J., Saczko, J., Mączyńska, J., Błasiak, P., Rossowska, J., & Rzechonek, A. (2018). Electroporation with cisplatin against metastatic pancreatic Cancer: In vitrostudy on human primary cell culture. *BioMed Research International*, *2018*, 1–12. https://doi.org/10.1155/2018/7364539

Miklavčič, D., Serša, G., Brecelj, E., Gehl, J., Soden, D., Bianchi, G., Ruggieri, P., Rossi, C. R., Campana, L. G., & Jarm, T. (2012). Electrochemotherapy: Technological advancements for efficient electroporation-based treatment of internal tumors. *Medical & Biological Engineering & Computing*, *50*(12), 1213–1225. https://doi.org/10.1007/s11517-012-0991-8

Mohamed, R. G., Elantabli, F. M., Abdel Aziz, A. A., Moustafa, H., & El-Medani, S. M. (2019). Synthesis, characterization, NLO properties, antimicrobial, CT-DNA binding and DFT modeling of Ni(II), Pd(II), Pt(II), Mo(IV) and Ru(I) complexes with NOS Schiff base. *Journal of Molecular Structure*, *1176*, 501–514. https://doi.org/10.1016/j.molstruc.2018.08.113

Neumann, E., Schaefer-Ridder, M., Wang, Y., & Hofschneider, P. H. (1982). Gene transfer into mouse lyoma cells by electroporation in high electric fields. *The EMBO Journal*, *1*(7), 841–845. https://doi.org/10.1002/j.1460-2075.1982.tb01257.x

Nithya, P., Rajamanikandan, R., Simpson, J., Ilanchelian, M., & Govindarajan, S. (2018). Solvent assisted synthesis, structural characterization and biological evaluation of cobalt(II) and nickel(II) complexes of Schiff bases generated from benzyl carbazate and cyclic

ketones. *Polyhedron*, *145*, 200–217. https://doi.org/10.1016/j.poly.2018.02.008

Qin, W., Long, S., Panunzio, M., & Biondi, S. (2013). Schiff bases: A short survey on an evergreen chemistry tool. *Molecules (Basel, Switzerland)*, *18*(10), 12264–12289. https://doi.org/10.3390/molecules181012264

Rahmouni, A., Souiei, S., Belkacem, M. A., Romdhane, A., Bouajila, J., & Ben Jannet, H. (2016). Synthesis and biological evaluation of novel pyrazolopyrimidines derivatives as anticancer and anti-5-lipoxygenase agents. *Bioorganic Chemistry*, *66*, 160–168. https://doi.org/10.1016/j.bioorg.2016.05.001

Rashad, A. E., Mahmoud, A. E., & Ali, M. M. (2011). Synthesis and anticancer effects of some novel pyrazolo[3,4-d]pyrimidine derivatives by generating reactive oxygen species in human breast adenocarcinoma cells. *European Journal of Medicinal Chemistry*, *46*(4), 1019–1026. https://doi.org/10.1016/j.ejmech.2011.01.013

Romeo, S., Sannino, A., Scarfì, M. R., Vernier, P. T., Cadossi, R., Gehl, J., & Zeni, O. (2018). ESOPE-equivalent pulsing protocols for calcium electroporation: An in vitro optimization study on 2 cancer cell models. *Technology in Cancer Research & Treatment*, *17*, 153303381878807. https://doi.org/10.1177/1533033818788072

Saad, F. A. (2014). Synthesis, spectral, electrochemical and X-ray single crystal studies on Ni(II) and Co(II) complexes derived from 1-benzoyl-3-(4-methylpyridin-2-yl) thiourea. *Spectrochimica Acta. Part A, Molecular and Biomolecular Spectroscopy*, *128*, 386–392. doi:0.1016/j.saa.2014.02.189 https://doi.org/10.1016/j.saa.2014.02.189

Şahin, Ö., Özdemir, Ü. Ö., Seferoğlu, N., Genc, Z. K., Kaya, K., Aydıner, B., Tekin, S., & Seferoğlu, Z. (2018). New platinum (II) and palladium (II) complexes of coumarin-thiazole Schiff base with a fluorescent chemosensor properties: Synthesis, spectroscopic characterization, X-ray structure determination, in vitro anticancer activity on various human carcinoma cell lines and computational studies. *Journal of Photochemistry and Photobiology. B, Biology*, *178*, 428–439. https://doi.org/10.1016/j.jphotobiol.2017.11.030

Sarı, Y., Gürses, C., Celepci, D. B., Keleştemur, Ü., Aktaş, A., Yüksel, Ş., Ateş, B., & Gök, Y. (2020). 4-Vinylbenzyl and 2-morpholinoethyl substituted ruthenium(II) complexes: Design, synthesis, and biological evaluation. *Journal of Molecular Structure*, *1202*, 127355. https://doi.org/10.1016/j.molstruc.2019.127355

Schneider, E., Hsiang, Y.-H., & Liu, L. F. (1990). DNA topoisomerases as anticancer drug targets. *Advances in Pharmacology*, *21*, 149–183. https://doi.org/10.1016/S1054-3589(08)60342-7

Shah, R. K., Abou-Melha, K. S., Saad, F. A., Yousef, T., Al-Hazmi, G. A. A., Elghalban, M. G., Khedr, A. M., & El-Metwaly, N. (2016). Elaborated studies on nano-sized homo-binuclear Mn(II), Fe(III), Co(II), Ni(II), and Cu(II) complexes derived from N_2O_2 Schiff base, thermal, molecular modeling, drug-likeness, and spectral. *Journal of Thermal Analysis and Calorimetry*, *123*(1), 731–743. https://doi.org/10.1007/s10973-015-4838-z

Tahir, M., Sirajuddin, M., Haider, A., Ali, S., Nadhman, A., & Rizzoli, C. (2019). Synthesis, spectroscopic characterization, crystal structure, interaction with DNA, CTAB as well as evaluation of biological potency, docking and molecular dynamics studies of N-(3,4,5-trimethoxybenzylidene)-2,3-dimethylbenzenamine. *Journal of Molecular Structure*, *1178*, 29–38. https://doi.org/10.1016/j.molstruc.2018.10.014

Tan, A., Kizilkaya, S., Kelestemur, U., Akdemir, A., & Kara, Y. (2020). The synthesis, anticancer activity, structure–activity relationships and molecular modelling studies of novel isoindole-1,3(2*H*)-dione compounds containing different functional groups. *Anti-Cancer Agents in Medicinal Chemistry*, *20*(11), 1368–1378. https://doi.org/10.2174/1871520620666200410080648

Turan, N., Buldurun, K., Alan, Y., Savci, A., Çolak, N., & Mantarcı, A. (2019). Synthesis, characterization, antioxidant, antimicrobial and DNA binding properties of ruthenium(II), cobalt(II) and nickel(II) complexes of Schiff base containing o-vanillin. *Research on Chemical Intermediates*, *45*, 3525–3540. https://doi.org/10.1007/s11164-019-03806-3

Vashi, K., & Naik, H. B. (2004). Synthesis of novel Schiff base and azetidinone derivatives and their antibacterial activity. *E-Journal of Chemistry*, *1*(5), 272–276. https://doi.org/10.1155/2004/158924

Vásquez, J. L., Ibsen, P., Lindberg, H., & Gehl, J. (2015). In vitro and in vivo experiments on electro chemotherapy for bladder cancer. *Journal of Urology*, *193*(3), 1009–1015. https://doi.org/10.1016/j.juro.2014.09.039

Yeğiner, G., Gülcan, M., Işık, S., Ürüt, G. Ö., Özdemir, S., & Kurtoğlu, M. (2017). Transition metal (II) complexes with a novel azo-azomethine Schiff base ligand: Synthesis, structural and spectroscopic characterization, thermal properties and biological applications. *Journal of Fluorescence*, *27*(6), 2239–2251. https://doi.org/10.1007/s10985-017-2166-3

Zhang, Y., Zhang, L., Liu, L., Guo, J., Wu, D., Xu, G., Wang, X., & Jia, D. (2010). Anticancer activity, structure, and theoretical calculation of N-(1-phenyl-3-methyl-4-propyl-pyrazolone-5)-salicylidene hydrazone and its copper(II) complex. *Inorganica Chimica Acta*, *363*(2), 289–293. https://doi.org/10.1016/j.ica.2009.08.017

Zielichowska, A., Daczewska, M., Saczko, J., Michel, O., & Kulbacka, J. (2016). Applications of calcium electroporation to effective apoptosis induction in fibrosarcoma cells and stimulation of normal muscle cells. *Bioelectrochemistry (Amsterdam, Netherlands)*, *109*, 70–78. https://doi.org/10.1016/j.bioelechem.2016.01.005

Zoubi, W. A. (2013). Biological activities of schiff bases and their complexes: A review of recent works. *International Journal of Organic Chemistry*, *03*(03), 73–95. https://doi.org/10.4236/ijoc.2013.33A008